COBEM 2023 27TH INTERNATIONAL CONGRESS OF MECHANICAL ENGINEERING

ABCM Brazilian Society of Mechanical Sciences and Engineering
27th ABCM International Congress of Mechanical Engineering
December 04-08, 2023, Florianópolis-SC, Brazil

COB-2023-1744
EFFECT OF PROCESS PARAMETERS ON THE PROPERTIES AND MICROSTRUCTURES OF CrMnFeCoNi COATINGS PRODUCED BY LASER CLADDING

Athos Fernandes Araujo
Cláudio Michel Poffo
Daniel Fonseca da Cunha
Catarina Meiko Hayashi
Felipe Martina Andre
Programa de Pós-Graduação em Ciência e Engenharia de Materiais - Universidade Federal de Santa Catarina - Campus Universitário – Bloco A do Depto. de EMC C.x. Postal 476 CEP.: 88.040-900 – Florianópolis
athos.araujo@ posgrad.ufsc.br
claudio.poffo@ufsc.br
daniel.cunha@ufsc.br
hayashi.h@posgrad.ufsc.br
felipe.martina@posgrad.ufsc.br

Renan Luiz Santiago
Universidade Federal de Santa Catarina - Campus Blumenau – João Pessoa Street, 2750 - Velha, Blumenau - SC, 89036-002CEP.: 88.040-900 – Florianópolis
renan.luiz.santiago@grad.ufsc.br

Manoel Kolling Dutra
Milton Pereira
LMP – Precision Engineering Laboratory – EMC – CTC - Universidade Federal de Santa Catarina Florianópolis CEP 88040-900 – Santa Catarina - Brasil
manoel.kolling@posgrad.ufsc.br
milton.pereira@ufsc.br

Abstract. *In this study, we assessed the impact of scanning speed and laser power parameters on the microstructure and microhardness of a coating comprised of a nearly equiatomic alloy consisting of high purity metallic powders of Cr, Mn, Fe, Co, and Ni. The deposition of the coating was accomplished using the laser cladding technique. We conducted a comprehensive analysis of the structural, mechanical, and microstructural properties of the resulting coatings after laser melting. To evaluate the mechanical strength of both the substrate and coatings, Vickers microhardness tests were performed. Optical microscopy was employed to identify regions with microstructural alterations and determine the percentage of dilution ratios. Additionally, SEM/EDS analysis was conducted to determine the chemical composition of the coating.*

Keywords: *high entropy alloys, laser cladding, characterization.*

1. INTRODUCTION

Opposing the traditional metallurgy that works with alloys with low numbers of components, new researchers have been trying to synthesize new alloys with new alloys mixing many metallic elements, each one in large proportions (Arif *et al.* 2021; Zhang *et al.* 2016).High entropy alloys (HEA) break the traditional design concept with a single main element and develop new ideas for the design of new alloys. Based on high entropy effect, lattice distortion effect, slow diffusion effect and cocktail effect (Tsai & Yeh, 2014; Yeh *et al.*, 2007). Among the main properties of HEA are excellent performance in low temperature toughness, high temperature stability and wear resistance (Arif *et al.*, 2021; Cantor *et al.*, 2004; Yeh *et al.*, 2004).

So far, magnetron sputtering, laser pulsed deposition, laser cladding, arc surfacing and other surface engineering technologies have been successfully employed to fabricate HEAs coatings (Lu *et al.* 2019; Song *et al.* 2019; Su *et al.* 2020; Zhang *et al.* 2017). Laser deposition techniques have emerged as an excellent alternative for producing coatings with better corrosion, oxidation and wear resistance properties. Among them, laser cladding (LC) has the advantages of high preparation freedom due to the characteristics of high energy density, high solidification rates, less heat effect on the substrate, good metallurgical bonding, less cracking and process automation (Arif *et al.*, 2021; Mukherjee *et al.*, 2021; L. Song *et al.*, 2016; C. Zhang *et al.*, 2021).

Energy density plays a crucial role in the laser cladding process, as the density increases, the interaction between the laser and the cladding material also intensifies. Resulting in more efficient melting of the material and stronger adhesion to the substrate. However, it is important to find a proper energy density balance to avoid unwanted effects such as porosity formation or substrate overheating. Energy density optimization is a complex task that requires specific knowledge about the materials involved, the desired coating properties and process parameters (Zhu *et al.*, 2021).

2. MATERIALS AND METHODS

The Materials and Methods section provides a detailed description of the experimental setup and procedures employed in this study to investigate the impact of scanning speed and laser power parameters on the microstructure and microhardness of a coating composed by metallic powders of Cr, Mn, Fe, Co, and Ni. This section outlines the materials used, the experimental techniques applied, and the data collection and analysis methods employed to achieve the research objectives. By presenting a comprehensive account of the methodology, this section aims to provide transparency and reproducibility of the experimental work, facilitating a clear understanding of the study's procedures and allowing for the validation of the obtained results. The following subsections elaborate on the materials selection, experimental setup, data acquisition, and statistical analysis performed in this investigation

2.1 Preparation of the coatings

As base material, a SAE1020 annealed steel plate measuring 100 x 50 x 10 mm was chosen. As a coating material, an equiatomic alloy of CrMnFeCoNi produced by mechanical alloying for 20 hours was used. The powder alloy was deposited on the steel plate in the form of 2 beads of 45 mm in length, 5 mm in width and 1 mm in height, as shown in Figure 1.

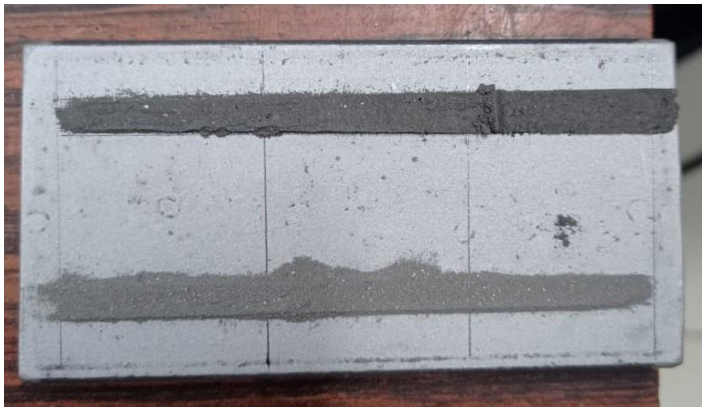

Figure 1. Powder alloy deposition.

Each bead was divided into three sections of 30 mm in length. For the first bead, it was decided to vary the laser power in each of the sections, keeping the scanning speed constant. In the second, the scanning speed was varied, keeping the laser power fixed. Laser input parameters are shown in Table 1 and Table 2.

Table 1. Parameters set for the Experiment 1.

Parameters	**Sample 1**	**Sample 2**	**Sample 3**
Power (W)	1500	2000	2500
Speed (mm/s)	5	5	5
Energy density (J/mm^2)	250	333	416

Table 2. Parameters set for the Experiment 2.

Parameters	**Sample 4**	**Sample 5**	**Sample 6**
Power (W)	1500	1500	1500
Speed (mm/s)	5	3,75	3
Energy density (J/mm^2)	250	333	416

A fiber laser system capable of operating at up to 10 kW with a protective argon atmosphere was used. The samples were moved by moving the table in XY under computer numerical control (CNC) and in both beads, the laser spot size is 850 µm, but was defocused to stay at 1200 µm.

2.2 Characterization of the coatings

The samples obtained were sectioned. The cross sections of the samples were mounted, sanded and polished. Subsequently, they were attacked with 2% Nital, followed by attack with an aqueous solution of 10% HF, 15% HCl and 25% HNO_3.

The microhardness profile was determined in a Vickers Microdurometer (DHTMVS-1000), with a load of 500 N and a dwell time of 10 s. Each sample was tested three times at the same horizontal line, and their values reported was an average of three measurements. The distance between measurements of 0.5 mm, with the first measurement close to the coating surface until reaching the steel substrate, as indicated in Figure 2.

The morphology and microstructure of the coatings was visualized using an Optical Microscope AxioVert.A1. The free software ImageJ was used to measure the penetrations of the fused alloy, as well as the zones where it was possible to identify microstructural changes. SEM/EDS was also used to identify and determine the chemical composition of the phases.

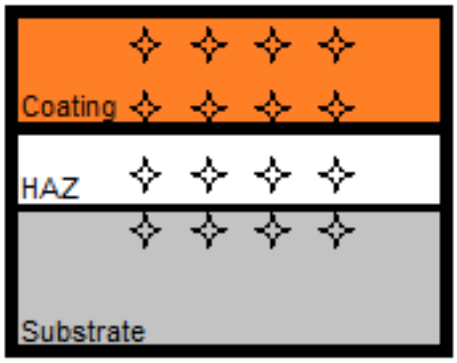

Figure 2. Distribution schematic of indentations for the microhardness test.

3. RESULTS AND DISCUSSION

3.1 Microhardness

Table 3 shows the results of microhardness for each parameter. It reveals that, as expected, the cladded coatings have higher micro hardness than that of 1020 substrate.

Table 3. Results of microhardness.

Regions	Fused Zone (HV)	σ	Heat Affected Zone (HV)	σ	Substrate (HV)	σ
Sample 1	403.6	22.9	345.2	50.9	198.6	5.6
Sample 2	425.6	32.2	329.7	48.4	198.3	6.7
Sample 3	430.2	20.0	317.5	16.5	180.0	15.8
Sample 4	406.9	27.8	350.8	35.6	185.4	35.1
Sample 5	417.2	26.1	370.5	13.0	193.9	26.5
Sample 6	348.7	44.8	273.4	33.8	183.4	8.1

It was possible to observe a direct relationship between laser power (samples 1, 2 and 3) and hardness. The increase in energy causes the fused zones to reach higher temperatures, and the regions closest to the substrate have higher cooling rates.

In samples where there was variation in the laser scanning speed (samples 4, 5 and 6) different behaviors occurred for each case. Between samples 4 and 5, it showed an increase in hardness with a decrease in speed. Possibly the value of the cooling rate is large enough to prevent grain growth and consequently a decrease in hardness. However, when it again decreased the speed, for sample 6, there was a reduction in microhardness. The low scanning speed allowed a slower heat exchange between the molten alloy and the substrate, promoting grain growth in the thermally affected zone and consequently decreasing hardness values.

3.2 Optical microscopy

Figures 3 and 4 show the optical microscopy of the sample cross section. The conditions corresponding to Tables 1 and 2, respectively.

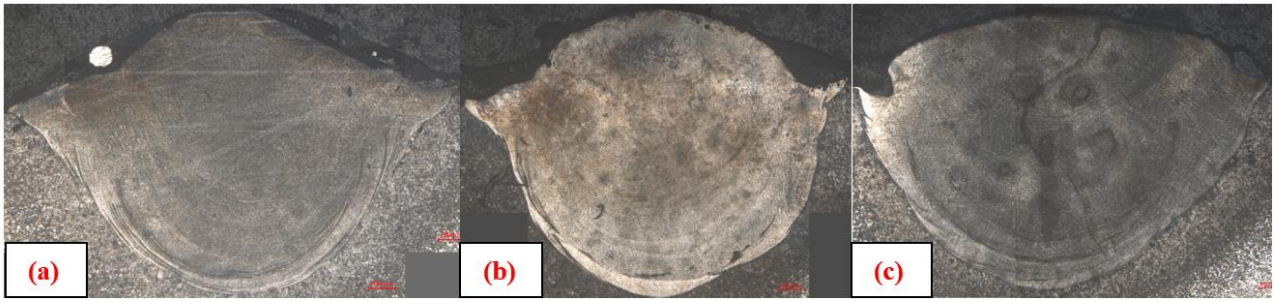

Figure 3. Cross section of the sample 1 (a), 2 (b) and 3 (c), 50x of magnification.

Figure 4. Cross section of the sample 4 (a), 5 (b) and 6 (c), 50x of magnification.

In the figure 5 is possible see the microstructure of the fused zone for the sample 1, similar structures are observed in all samples. The micrograph indicates that the coating is dense enough, free of cracks and with few pores. The microstructure of the cladding zone (concave region) is mainly constituted by fine, non-oriented and equiaxed grains. It is also possible to observe that a curved line at the interface of the molten alloy and the substrate, as opposed to a straight line, indicates a good metallurgical bond between the coating and the base material. Due to the fast melting-solidification dynamics during the laser cladding process, the temperature difference (ΔT) is very high, as well as the nucleation rate which is much higher than the crystal growth rate. Thus, the columnar grain growth direction is perpendicular to the interface zone due to the rapid directional solidification, typical of the laser cladding process (Vyas *et al.*, 2020).

Figure 5. Microstructure of the fused zone sample 1, 200x magnification.

Using the ImageJ software, it was possible to measure the sizes of the merged zones and the HAZ of the samples. And with these dimensions find the dilution rates given by Equation (1).

$$\eta = h/(h + H)x100 \quad (1)$$

Where η, h, H are the dilution rate, height and deep, respectively. Figure 6 shows a schematic diagram of how the measurements were carried out. Table 4 shows the obtained values.

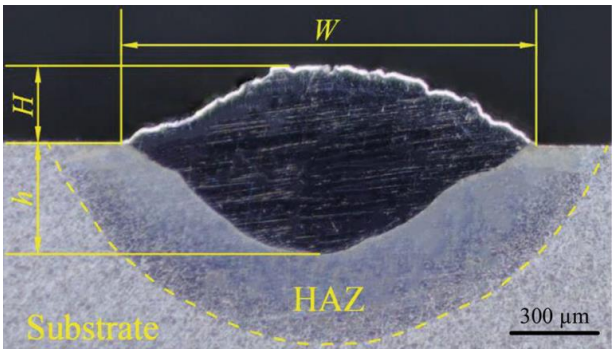

Figure 6. Schematic diagram of the measurements for a laser cladded coating (Huang *et al.*, 2022).

Table 4. Dimensions and dilution rate.

Sample	Height (H) (µm)	Depth (h) (µm)	Width (W) (µm)	HAZ length (L_{HAZ})(µm)	Dilution rate (η) (%)
Sample 1	630.0	1430.3	3249.9	337.7	69.4
Sample 2	744.6	1833.2	3456.1	376.5	71.1
Sample 3	640.3	1901.6	3860.8	383.4	74.8
Sample 4	687.9	1397.6	3143.4	316.0	67.0
Sample 5	405.6	1759.8	3341.4	263.7	81.3
Sample 6	867.0	1559.1	3439.2	249.2	64.3

The values for the HAZ lengths were given through averages of three different regions. The HAZ lengths seem to be directly related to the energy density values. Among the samples where there was a change in laser power, the one with the highest power had the longest length, due to the greater amount of heat conducted to the substrate. As for samples where there was variation in speed, the one with the greatest length was the condition with 3 mm/s. It happened due to the lower scanning speed, which hindered thermal exchange, changing the morphology of nearby grains.

3.3 SEM/EDS

Figure 7 shows the SEM images for sample 1, 3 and 6. It is possible to visualize the grain boundaries and the presence of pores. Comparing the samples, it is noticed that with the increase in energy densities, the amount of pores decreases. Again, using the ImageJ software, it was possible to estimate the average grain sizes for these three samples. The grains of sample 1 measure approximately 45.2 µm^2, in sample 3 the size is 47.9 µm^2 and in sample 6 48.7 µm^2. With these results, it is not possible to relate the grain sizes with the laser operating parameters.

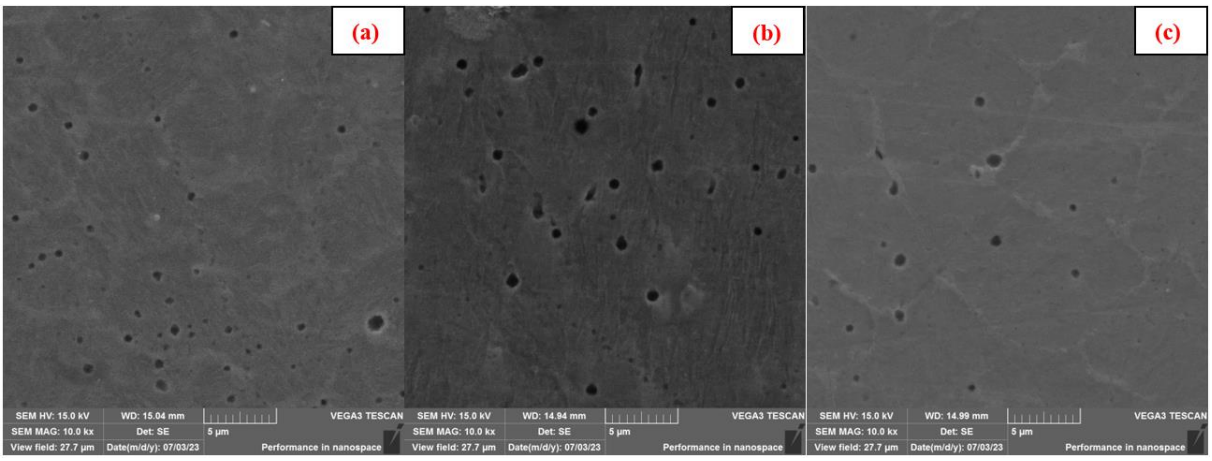

Figure 7. SEM images of sample 1 (a), 3 (b) e 6 (c).

Figure 7 shows the chemical composition of sample 6 obtained by EDS, similar compositions were observed in the other samples. The presence of a single phase in the cladding region associated with the chemical composition found, it can be assumed that the previously deposited high entropy alloy was completely melted and incorporated into the substrate. Producing an alloy of Fe with the elements Ni, Cr, Co, Mn dispensed by the matrix. This hypothesis can also be corroborated when considering the high percentages of dilution and penetration shown in Table 4. On the other hand, for similar laser powers, larger focal spot diameters were applied, decreasing the energy density at the spot. Thus, melting of the alloy is guaranteed, but an increase in the depth of the fused zone as well as mixing with the substrate is avoided (Jiang et al. 2019; Liu *et al.* 2019; Liu et al. 2022).

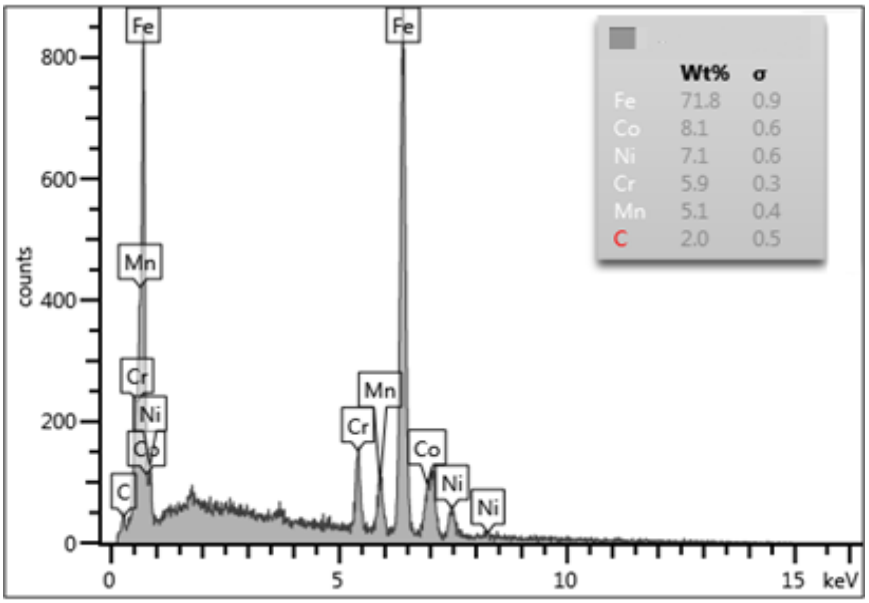

Figure 8. Chemical composition obtained by EDS for sample 6.

4. CONCLUSIONS

In this work it was presented the effects of varying scanning speed and laser power on the cladding of a high entropy alloy pre-deposited on a SAE 1020 steel substrate.

The fused zones presented microhardness 2 times greater than the substrate. This increase is mainly due to the new alloy being added and mixed with the substrate. However, in HAZ the increase was on average 1.7 times greater, in this region the main mechanism was the recrystallization of grains due to thermal input followed by rapid cooling that refined the size of nearby grains.

The percentages of dilution obtained show that there was a great dilution of the alloy in the substrate. The high penetration allowed the melting of the alloy, and its dilution in the substrate, actually occurring the laser surface alloying process, which can be confirmed by the absence of other phases and structures and by the chemical composition obtained by the SEM/EDS.

For the production of coatings through laser cladding, a transition zone formed by the mixture between the substrate and the alloy is expected, followed by a region formed only by the deposited material. Such a cladding effect could be achieved by working with larger focus diameters which would affect the energy density relationships.

Despite the complications, with the parameters used it was still possible to melt the alloy and generate a cast zone with good metallurgical bonding, solidification structure and uniform composition.

5. ACKNOWLEDGEMENTS

The work presented here was conducted at the Universidade Federal de Santa Catarina, in the UFSC – Blumenau laboratories and the Precision Engineering Laboratory (LMP-LASER) in Florianópolis. We also thank the members of GESMat, for all their support. This study was also financed by the National Council for Scientific and Technological Development (CNPq) and Coordenação de Aperfeiçoamento de Pessoal de Nível Superior (CAPES).

6. REFERENCES

Arif, Z. U., Khalid, M. Y., ur Rehman, E., Ullah, S., Atif, M., & Tariq, A. (2021). A review on laser cladding of high-

entropy alloys, their recent trends and potential applications. *Journal of Manufacturing Processes*, *68*(PB), 225–273.

Cantor, B., Chang, I. T. H., Knight, P., & Vincent, A. J. B. (2004). Microstructural development in equiatomic multicomponent alloys. *Materials Science and Engineering A*, *375–377*(1-2 SPEC. ISS.), 213–218.

Huang, Y., Hu, Y., Zhang, M., Mao, C., Wang, K., Tong, Y., Zhang, J., & Li, K. (2022). Multi-Objective Optimization of Process Parameters in Laser Cladding CoCrCuFeNi High-Entropy Alloy Coating. *Journal of Thermal Spray Technology*, *31*(6), 1985–2000.

Jiang, Y. Q., Li, J., Juan, Y. F., Lu, Z. J., & Jia, W. L. (2019). Evolution in microstructure and corrosion behavior of AlCoCrxFeNi high-entropy alloy coatings fabricated by laser cladding. *Journal of Alloys and Compounds*, *775*, 1–14.

Liu, J., Liu, H., Chen, P., & Hao, J. (2019). Microstructural characterization and corrosion behaviour of AlCoCrFeNiTi x high-entropy alloy coatings fabricated by laser cladding. *Surface and Coatings Technology*, *361*(November 2018), 63–74.

Liu, S. S., Zhang, M., Zhao, G. L., Wang, X. H., & Wang, J. F. (2022). Microstructure and properties of ceramic particle reinforced FeCoNiCrMnTi high entropy alloy laser cladding coating. *Intermetallics*, *140*(September 2021), 107402.

Lu, T. W., Feng, C. S., Wang, Z., Liao, K. W., Liu, Z. Y., Xie, Y. Z., Hu, J. G., & Liao, W. B. (2019). Microstructures and mechanical properties of CoCrFeNiAl0.3 high-entropy alloy thin films by pulsed laser deposition. *Applied Surface Science*, *494*(July), 72–79.

Mukherjee, S., Dhara, S., & Saha, P. (2021). Enhanced corrosion , tribocorrosion resistance and controllable osteogenic potential of stem cells on micro-rippled Ti6Al4V surfaces produced by pulsed laser remelting. *Journal of Manufacturing Processes*, *65*(July 2020), 119–133.

Song, B., Li, Y., Cong, Z., Li, Y., Song, Z., & Chen, J. (2019). Effects of deposition temperature on the nanomechanical properties of refractory high entropy TaNbHfZr films. *Journal of Alloys and Compounds*, *797*, 1025–1030.

Song, L., Zeng, G., Xiao, H., Xiao, X., & Li, S. (2016). Repair of 304 stainless steel by laser cladding with 316L stainless steel powders followed by laser surface alloying with WC powders. *Journal of Manufacturing Processes*, *24*, 116–124.

Su, Y., Liang, X., Liu, Y., & Dai, Z. (2020). Effect of Ti Addition on the Microstructure and Property of FeAlCuCrNiMo0.6 High-Entropy Alloy. *Acta Metallurgica Sinica (English Letters)*, *33*(7), 957–967.

Tsai, M. H., & Yeh, J. W. (2014). High-entropy alloys: A critical review. *Materials Research Letters*, *2*(3), 107–123.

Vyas, A., Menghani, J., & Natu, H. (2020). Metallurgical and mechanical properties of laser cladded AlFeCuCrCoNi-WC10 high entropy alloy coating. *International Journal of Engineering, Transactions A: Basics*, *33*(7), 1397–1402.

Yeh, J. W., Chang, S. Y., Hong, Y. Der, Chen, S. K., & Lin, S. J. (2007). Anomalous decrease in X-ray diffraction intensities of Cu-Ni-Al-Co-Cr-Fe-Si alloy systems with multi-principal elements. *Materials Chemistry and Physics*, *103*(1), 41–46.

Yeh, J. W., Chen, S. K., Lin, S. J., Gan, J. Y., Chin, T. S., Shun, T. T., Tsau, C. H., & Chang, S. Y. (2004). Nanostructured high-entropy alloys with multiple principal elements: Novel alloy design concepts and outcomes. *Advanced Engineering Materials*, *6*(5), 299–303.

Zhang, C., Chen, S., Zhou, L., Wei, M., Liang, J., Liu, C., & Wang, M. (2021). Effects of carbon fibers on the microstructure and properties of laser cladding 24CrNiMoY alloy steel. *Journal of Manufacturing Processes*, *62*(December 2020), 337–347.

Zhang, M., Zhou, X., Yu, X., & Li, J. (2017). Synthesis and characterization of refractory TiZrNbWMo high-entropy alloy coating by laser cladding. *Surface and Coatings Technology*, *311*, 321–329.

Zhang, Y., Koch, C. C., Ma, S. G., Zhang, H., & Pan, Y. (2016). Fabrication routes. *High-Entropy Alloys: Fundamentals and Applications*, 151–179. Springer International Publishing.

Zhu, L., Xue, P., Lan, Q., Meng, G., Ren, Y., Yang, Z., Xu, P., & Liu, Z. (2021). Recent research and development status of laser cladding: A review. *Optics and Laser Technology*, *138*(January), 106915.

RESPONSIBILITY NOTICE

The authors are the only responsible for the printed material included in this paper.